Electrochemically-grown Chloride-free Cu₂O Nanocubes Favorably Electroreduce CO₂ to Methane: The Interplay of Appropriate Electrochemical Protocol

Stefan Popović*[a,b], Mohammed Azeezulla Nazrulla[a], Primož Šket[c], Khaja Mohaideen Kamal[d], Blaž Likozar[d], Luka Suhadolnik[e], Luka Pavko[a], Angelja Kjara Surca[a], Marjan Bele[a], Nejc Hodnik*[a,b]

[a] Department of Materials Chemistry, National Institute of Chemistry, Hajdrihova 19, 1000 Ljubljana, Slovenia
[b] University of Nova Gorica, Vipavska 13, 5000 Nova Gorica, Slovenia
[c] Slovenian NMR Center, National Institute of Chemistry, Hajdrihova 19, 1000 Ljubljana, Slovenia
[d] Department of Catalysis and Chemical Reaction Engineering, National Institute of Chemistry, Hajdrihova 19, 1000 Ljubljana, Slovenia
[e] Department of Chemical and Pharmaceutical Sciences, University of Trieste, via L. Giorgieri 1, 34127 Trieste, Italy

Abstract: Nowadays, electrochemical CO_2 reduction reaction (CO_2RR) to value-added products represents one of the major challenges in electrocatalysis. Copper-based nanocubes (Cu NCs) have been proposed as the front-runner's catalyst for the production of C_{2+} products at the industrial level. However, their selectivity (C_1 vs. C_2 product distribution) is rather complex depending on the dynamic structural transformations, the presence of mixed Cu^+/Cu^0 states, the microenvironment, and nanocatalyst-support interactions. Commonly, electrochemically-grown Cu NCs are prepared in the presence of chlorides that acts as a shaping agent. In this study, an optimized electrodeposition method for the synthesis of Cl^--free Cu_2O nanocubes on a glassy carbon substrate with uniform size, shape, and loading is established. The successful preparation of chloride-free cuprous oxide nanocubes (Cu_2O NCs) was confirmed with X-ray diffraction (XRD), Raman spectroscopy, scanning electron microscopy (SEM), and X-ray photoelectron spectroscopy (XPS) analyses. We report how the electrochemical double-layer capacitance (EDLC) method for electrochemical surface area (ECSA) determination with(out) subsequent return to the open-circuit potential (OCP) conditions before electrolysis influences the CO_2RR activity/selectivity. When Cu_2O NCs are subjected to the EDLC method (often considered a non-invasive method) and exposed to the OCP before electrolysis, they become active for methane (CH_4) formation. Moreover, the influence of the potential window width (i.e. 200 and 400 mV) in which the EDLC-ECSA is employed and its correlations with the selectivity is presented. We underline the importance of the ECSA determination method and OCP on/off state as a triggering factor for reactivity/selectivity of particular Cu_2O NCs for CO_2RR and further emphasize the reconstructive nature of Cu_2O NCs under CO_2RR relevant conditions.

KEYWORDS: *Copper nanocubes, CO₂ reduction, selectivity, methane, support effect*

1. Introduction

Unfolding the energy, together with the climate crisis, once again warned that investment in the cutting-edge science of electrochemical technologies for energy storage and conversion will be of paramount importance to sustain energy demands. In the last two decades, tremendous efforts have been undertaken to develop these technologies to become independent of current energy derivatives (coal, gas, oil). Until now the majority did not reach a cost-effective commercial level.[1] Despite the overoptimistic assertion that electrocatalytic carbon dioxide reduction reaction (CO_2RR) could potentially contribute to CO_2 removal from the atmosphere, the technology has sparked interest in sustainable means of converting CO_2 into value-added products, ideally powered by renewable energy.[2,3] The main hurdle in the process remains the "under-performance" of the electrocatalysts. Copper and copper-based materials are the only ones that can convert CO_2 to multicarbon products at a decent yield.[4] Among the complex interplay of various Cu-based catalyst parameters (morphology,

composition, oxidation state, shape, size, interparticle distance, loading, etc.) to improve the CO_2RR reactivity, the shape effect has attracted significant interest due to the tunable approach toward selectivity of certain facets.[5] In several well-studied single-crystal copper surfaces, certain facets provided favorable product selectivity. As a result of a significantly lower CO dimerization energy barrier, surfaces with abundant Cu(100) have been shown to selectively reduce CO_2 to C_2H_4. Likewise, it has been shown that Cu(111) is more selective toward CH_4.[6,7] Subsequently, the researchers have been trying to transfer this knowledge of single-crystal studies to the nanoparticles and synthesize shaped-like nanocatalysts with abundant particular facets.

Inline, cube-shaped copper (Cu NCs) nanoparticles with Cu(100)-rich surfaces have been recognized in the CO_2RR community as the propitious catalyst for the production of ethylene (C_2H_4) for future industrial applications.[8–12] Among various preparation methods for the synthesis of shaped nanoparticles[5], electrodeposition emerged as a prominent method because it is inexpensive, quick, requires simple equipment, and permits the precise tuning of electrochemical parameters for the generation of versatile self-supported nanostructures.[13] A group led by prof. Roldan Cuenya studied in detail the growth dynamics and morphological evolution of Cu_2O NCs using pulse-electrodeposition wherein nanocubes are grown in chloride-containing electrolytes. Moreover, the authors also reported the reactivity of electrochemically-grown Cu_2O NCs and their complex dynamic degradations behavior under CO_2RR-relevant conditions.[9,12,14] Grosse *et al.*[9] emphasized the support effect as one of the crucial factors for the determination of the product selectivity for the Cu NCs. Copper cubes on copper foil predominantly produce C_{2+} products, while copper cubes on carbon support tend to be more selective for C_1 products. Early works on Cu NCs towards enhancing activity/selectivity have neglected copper's reconstructive nature, focusing only on the as-prepared morphologies.[8,15,16] This has overshadowed the dynamics of the reconstruction as one of the most important steps to gain more insight into the structure-performance relationship. The Cu NCs have been proposed to undergo reconstruction due to the different reaction factors such as applied bias[17], CO_2RR intermediate-related adsorbates[18], local pH[19], etc. Lately, numerous in situ/operando studies have been devoted to the in-depth understanding of its influence on catalytic active sites, which is one of the most unclear and debatable topics for CO_2RR.[20,21] Most recently it has been shown that Cu surfaces are surprisingly stable under highly reducing conditions, thus, the reasonable explanation for the structural evolution can be described as sometimes unintentional surface oxidation and subsequent anisotropic reduction accompanied by the processes such as dissolution/redeposition.[22–24]

Further development of in-situ/operando techniques will be pivotal to gaining a clearer picture of the dynamic reconstruction and identifying catalytic active sites during CO_2RR.[25,26] As a result of all of the above, Cu(100) surface cannot be considered as the only determining factor for C_{2+} product formation, but rather there exists a synergism between dynamic structural transformations[27], and the presence of mixed Cu^+/Cu^0 oxidation states[28], microenvironment[25], and nanocatalyst-support interactions[9]. The reconstructive nature of Cu-based catalysts imposes one more obstacle to accurately and properly validating the catalyst's intrinsic activity, which is, the electrochemical surface area determination (ECSA). As the crucial figure of merit for accurate assessment of CO_2RR-current density, ECSA has often failed to be determined in a non-invasive and non-destructive manner. Few studies stress the importance of measuring ECSA in a minimally invasive, time-resolved, and destructive manner for a valid comparison of the catalyst's intrinsic activity, however, this remains elusive.[12,29,30] While employing statistical methods such as ex-situ SEM imaging[9] and AFM measurements[31] for the active surface area determination, always rises a question of reliability. The underpotential deposition (UPD) of Pb on copper acts destructively (most likely quasi-irreversible) by impurity presence.[32,33] Currently, one of the most popular, supposedly non-destructive, and widespread methods for ECSA determination in the CO_2RR community is the electrochemical double-layer capacitance (EDLC) method, often considered reliable for metal oxide that has high electrical conductivity.[34] However, in this study, we show that the EDLC-ECSA determination method such as method indeed affects catalysts' properties. It behaves as an electrochemical "activation protocol"

that boost the activity/selectivity of Cu NCs. Meticulously, we present an optimized pulse-alternating electrochemical protocol to produce Cu_2O- nanocubes (Cu NCs) with uniform size, shape, and loading. We for the first time demonstrate that, by tuning the stirring rate of the solution, reproducible Cu NCs can be synthesized in a 10 mM $CuSO_4$ electrodeposition bath in the absence of Cl^- ions, which were emphasized in the literature to be a critical additive for shaping Cu nanostructures and were shown to affect their selectivity.[14] We show that the addition of Cl^- is unnecessary to obtain Cu-based cubic-shaped nanoparticles and prove that the synthesized Cu-based NCs are indeed made out of cuprous oxide (Cu_2O). The electrocatalytic performance of as-prepared Cu_2O NCs on glassy carbon substrate showed no CO_2RR activity. Furthermore, the samples that underwent the EDLC-ECSA determination without subsequent return to OCP predominantly produced H_2. Interestingly, when the Cu-based NCs underwent the protocol in the form of a double-layer capacitive cycling method for the determination of ECSA, often considered a non-invasive method, before CO_2RR in combination with exposure to the OCP, they become active for methane formation. We also present the influence of different ECSA potential windows on the activity/selectivity and reveal the catalyst's morphological evolution before and after CO_2RR to gain newer insights into the structure-activity and structure-stability relationships of Cu-based systems.

2. Experimental Section
2.1. Chloride-free Electrodeposition of Cu_2O NCs

Among the various technologies for the synthesis of copper-based nanocatalysts[35], electrodeposition stands out as a powerful synthesis method with some major advantages such as 1) good adhesion of the deposits; 2) the absence of organic surfactants usage; 3) the usage of inorganic »shaping-agents« to tune catalysts shape.[14,36] Standing with the latter one, it is commonly accepted that chloride ions (Cl^-) in the precursor solution encourage nanocube formation, both with nucleation of the Cu_2O cubes and the stabilization of the Cu {100} facets. The extensive studies on electrodeposition of Cu NCs have emphasized that the concentration of Cl^- "had the most drastic effect on the catalyst size distribution and coverage". Moreover, the benchtop method for the electrodeposition of Cu NCs on glassy carbon substrates has been established through the so-called pulse-alternating method.[36] In this study, we posit the pulse-alternating electrochemical protocol in 10 mM $CuSO_4$ electrodeposition solution without the addition of chlorides to produce a uniform shape, size, and loading of Cu_2O NCs. Figure 1, Supplementary note 1, and Figures S1-S7 provide an in-depth description of the experimental procedure and optimization of the synthesis.
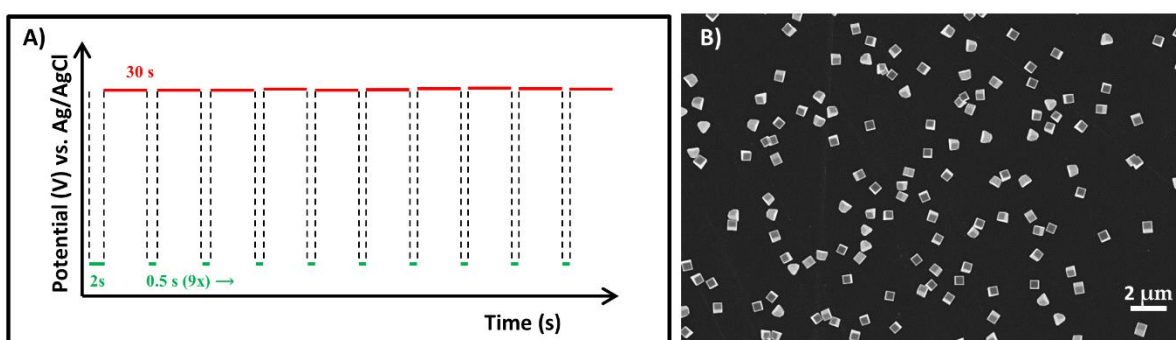

Figure 1. A) Pulse-alternating electrochemical protocol for electrodeposition of Cu_2O NCs. 10 mM $CuSO_4$ electrodeposition solution and stirring rate of 500 rpm are used for optimized synthesis. In total, 10 reductive pulses consisted of a first pulse of 2 s and 9 consecutive pulses of 0.5 s whereas the 30s-long oxidative pulses were selected; B) SEM micrograph of as-prepared Cu NCs.

3. Results and discussion
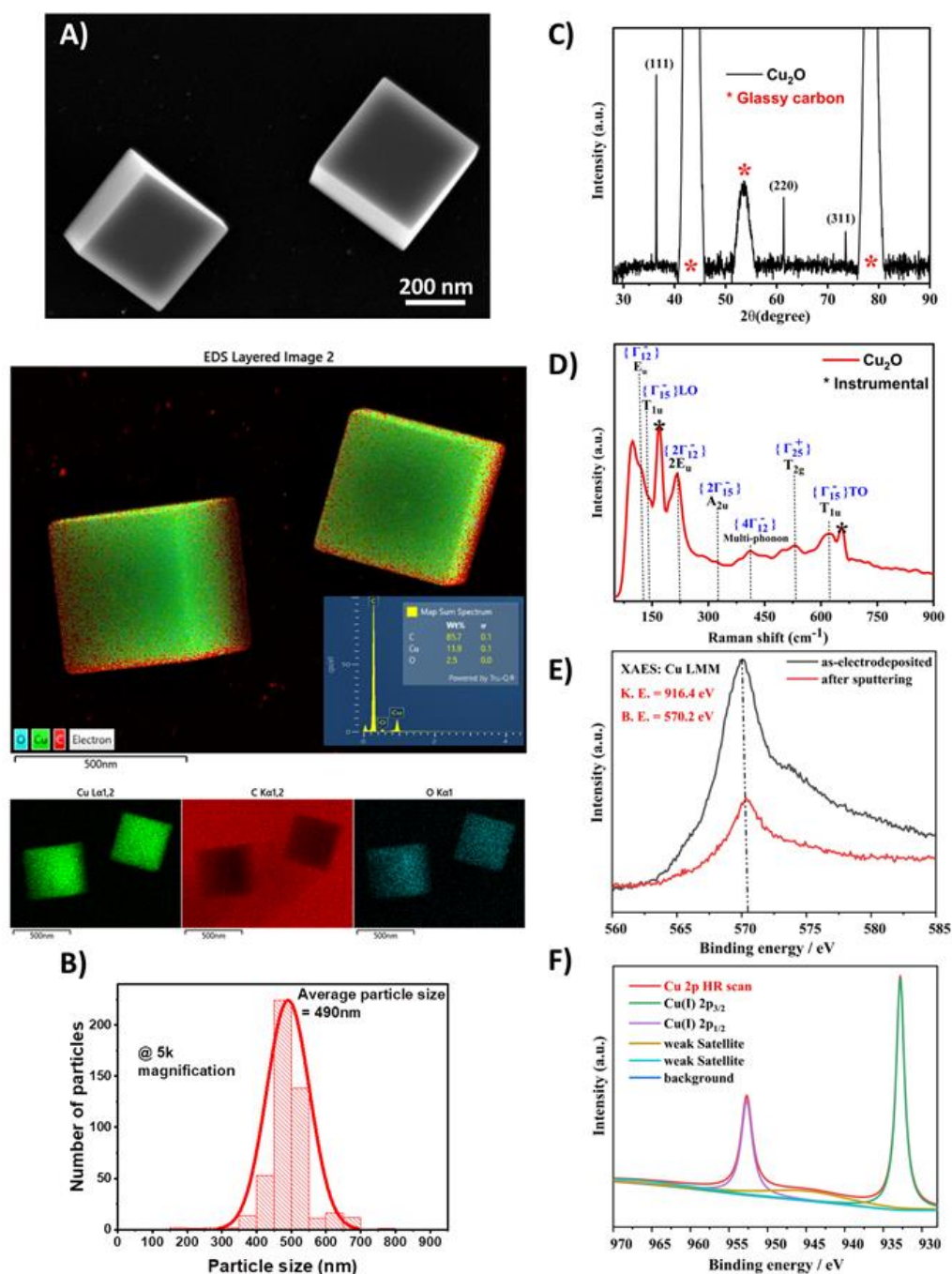
3.1. Characterization of as-prepared Cu NCs

Figure 2. A) Scanning electron microscopy (SEM) images of as-prepared Cu-based NCs with corresponding mapping EDX image and inset of quantitative map spectrum; B) Particle size distribution of as-prepared Cu NCs extracted from the 5k magnification SEM image with peak for average particle size at 490nm (Image J software); C) X-ray diffraction (XRD) pattern with assigned Cu2O diffraction peaks excluded from glassy carbon signal as support (marked); D) Ex-situ Raman spectroscopy data of as-prepared Cu NCs with assigned vibrational modes (*-instrumental band); E) Cu LMM XAES spectra with the peak at 570.2 eV of argon sputtered as-prepared Cu NCs F) XPS spectra of an argon-sputtered as-prepared sample of Cu 2p region.

The morphology of self-supported, chloride-free as-prepared Cu2O nanocubes on a glassy carbon substrate is characterized by high-resolution scanning electron microscopy (HR-SEM), and the corresponding well-defined cubic shapes are shown in Figure 2. A with the additional mapping images

of energy dispersive X-ray analysis (EDX) to confirm the elemental composition. The complete particle size distribution analysis for the optimized electrochemical protocol (Figure 1) is shown in Figure S5 with tabulated average particle size and loading for three independent samples. Hereby, the representative particle size distribution analysis is presented in Figure 2. B with the average particle size at the value of (490 ± 80) nm. To have a comparable number of 400-500 particles each time (in a given/certain area), the magnification of SEM images for the particle size distribution analysis was 5000. In further text, the particle size of Cu NCs will be denoted as "500nm". X-ray diffraction (XRD) was obtained to further confirm the composition of as-prepared Cu-based NCs. Figure 2. C shows the XRD pattern of Cu NCs which corroborates that electrochemically-grown Cu nanocubes are composed of pure Cu_2O without any metallic phase. The corresponding diffraction peaks for Cu_2O are assigned as (111), (220), and (311) at diffraction angles of 36.6°, 61.3°, and 73.5°, respectively. Looking at the reference of Cu and Cu_2O, the diffraction peak at 73.5° might be assigned either as Cu(220) or Cu_2O(311). Further, the absence of diffraction peaks for Cu(200) and Cu(311) at 50.4° and 89.9°, respectively infers that as-synthesized Cu NCs belong to the Cu_2O phase. Nevertheless, the intensity of the diffraction peak at 61.3°, for the above-mentioned Cu_2O(220), is 1.5-fold higher than that of the peak at 73,5°, which is a good correlation with Cu_2O reference patterns.[37] The expected signal of higher-order Cu_2O(100)-rich surface at Cu-based NCs, namely Cu_2O(200), overlapped with the signal of glassy carbon at 42,6°. The Raman spectrum of as-prepared Cu NCs is shown in Figure 2. D. Starting from the lowest Raman shift, a peak at 110 cm^{-1} and 141 cm^{-1} (longitudinal optical), assigned to the E_u and T_{1u} symmetry, correspond to the rotations of Cu tetrahedra around their centers in the Cu_2O lattice.[38] A Raman mode near 217 cm^{-1} known as the second-order mode of 110 cm^{-1} is also observed. A small hump near 405 cm^{-1} can be associated with a fourth-order overtone of Cu_2O.[39] Moreover, the peak at 529 cm^{-1} related to the only Raman-active mode of T_{2g} symmetry, consists of the out-of-phase motion of the two oxygen sublattices to each other with the copper sublattice remaining fixed. In addition, the peak at 620 cm^{-1} is IR-allowed transverse optical mode is also seen. Nonetheless, we did not observe any characteristic bands of the cupric oxide (CuO) phase in the Raman spectrum nor any diffraction peaks corresponding to CuO.

Despite ascertaining the as-electrodeposited nanocubes with Cu_2O-phase from ex-situ XRD and Raman measurements, further confirmation of the Cu_2O composition is provided by x-ray Auger electron spectroscopy (XAES). Figure 2. E shows Cu LMM Auger electron spectra (XAES) acquired from the argon-sputtered and as-prepared sample (Supplementary Note 2). The peak at 570.2 eV binding energy corresponds to the Cu_2O phase in argon-sputtered and as-prepared samples, which is in agreement with the x-ray photoelectron spectroscopic (XPS) measurements of the Cu 2p region where Cu $2p_{3/2}$ and Cu $2p_{1/2}$ are positioned at 932.84 and 952.7 eV, respectively. Since XPS is the surface-sensitive technique, we found that the shake-up satellites in as-prepared Cu NCs (without ion-sputtering) contain Cu^{2+} species on the surface. The satellite features at 933.5 and 943 eV correspond to the Cu(II) which we ascribed to partial near-surface oxidation of the already confirmed Cu_2O bulk structure (Figure S8). However, the absence of such features in argon-sputtered samples additionally indicates that the rest of the nanocubes (towards bulk) are pure Cu_2O-phase (Figure 2 F). Further, the modified Auger parameter (MAP) for as-electrodeposited and argon-sputtered copper nanocubes is found to be 1849.2 ($\pm$ 0.1) eV. It is evident from this MAP value that the chemical state of copper in the as-electrodeposited copper nanocubes is Cu(I) which is corresponding to the pure Cu_2O phase. To sum up, even though the electrodeposition method from the Cu^{2+}-rich electrolyte intuitively should produce metallic copper state Cu NCs ($Cu^{2+}+2e^{-}\rightarrow Cu^{0}$), the pulse-electrodeposition protocol consisted of, time-wise, mostly oxidative generation pulses (red pulse at Figure 1) at open-circuit potential (OCP), had two implications. The first one is that the final composition of bulk Cu- based NCs is Cu_2O and secondly, an oxidative period also served as the regime for the dissolution of non-cubic shapes.[36]
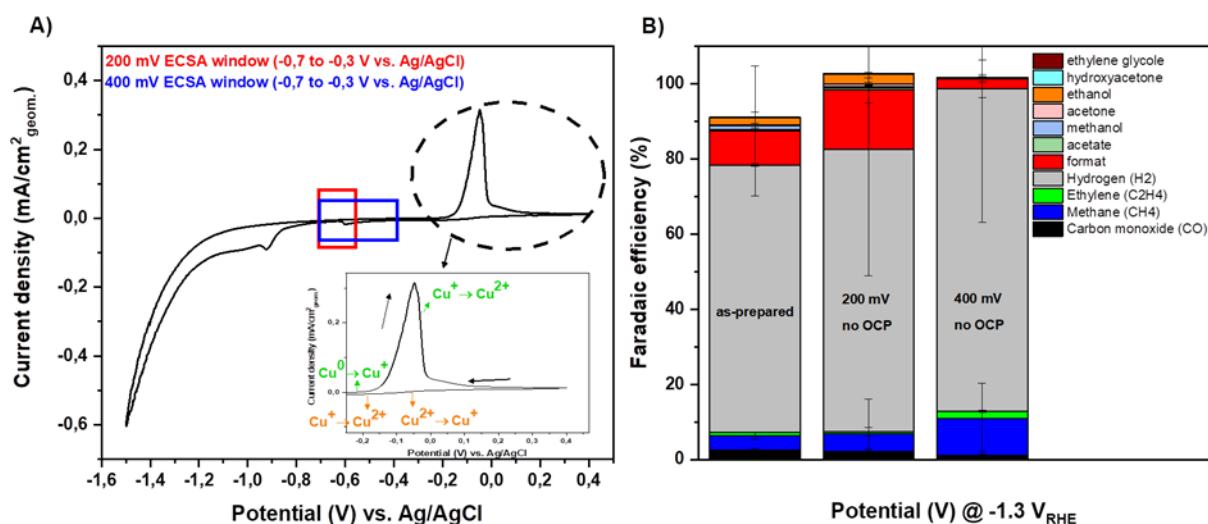
Figure 3. A) Cyclic voltammogram of the as-prepared Cu NCs with labeled potential windows used for ECSA from -1.5 to 0.4 V vs. Ag/AgCl with 5 mV/s scan rate. Change of oxidation states of copper during CV is assigned according to the in-situ analysis of Timoshenko *et al.*[40]; B) Faradaic efficiency for the inactivity of the Cu NCs is based on the "pre-treatment" viz, as-prepared, Cu NCs- NOOCP200 and Cu NCs- NOOCP400 samples at -1.3 V vs. RHE for 1h of electrolysis (no subsequent return to OCP between EDLC-ECSA determination method and CA measurements).

3.2. Electrocatalytic CO₂RR activity

The electrocatalytic measurements of electrochemically-grown Cu-based NCs were performed in a custom-made sandwich-type cell (Supplementary note 3). The as-prepared Cu-based NCs were tested in CO_2-saturated 0.1M $KHCO_3$ (pH=6.8) at various potentials (-1.1 to -1.4 V_{RHE}) with appropriate gaseous and liquid product detection/quantifications (Supplementary note 5). The electrocatalytic activity of Cu-based NCs under different electrochemical protocols is examined at various potentials. However, the estimation of the electrochemical surface area (ECSA) for the as-prepared Cu-based NCs remains elusive, even though ECSA assessment can be done through SEM statistical approach34 (Figure S5), further catalyst's intrinsic activity evaluation is practically inaccessible. We chose and stress the importance of the often assumed »non-invasive« double-layer capacitance method for ECSA determination and correlate its influence on the CO2RR activity/selectivity with(out) subsequent return to open-circuit potential (OCP) between EDLC-ECSA and chronoamperometric (CA) measurements. Figure 3. A shows the cyclic voltammogram of as-assembled and as-prepared Cu-based NCs with corresponding oxidation and reduction peaks. Accordingly, we chose two potential windows for ECSA determination inside the double-layer capacitance region where no Faradaic processes are present. The two potential windows for ECSA determination used in the study are 200 mV (-0.7 to -0.5 V vs. Ag/AgCl) and 400 mV (-0.7 to -0.3 V vs. Ag/AgCl) as depicted in the graph Figure 3. A. It is noteworthy, that for each independent electrolysis measurement the EDLC-ECSA determination method was repeated twice before electrolysis (CA) measurement at 5 different scan rates (20, 50, 100, 200, and 300 mV/s). Therefore, in the further text, we denote the Cu-based NCs samples as »Cu NCs-NOOCP200« and »Cu NCs-NOOCP400« when there is no return to OCP in-between double-layer cycling (ECSA determination method) and chronoamperometry measurements. Figure 3. B) represents the CO₂RR Faradaic efficiency of three different »pre-treated« Cu-based NCs samples at -1.3V vs. RHE. Adequately, throughout the optimization of the electrodeposition method, we achieved a uniformity of loading to have the same ECSA each time (Figure S5) so the as-prepared Cu-based NCs were imposed directly to the reductive potential without further measuring ECSA. Surprisingly, as-prepared Cu-based NCs showed almost no activity towards CO₂RR with negligible production of CH₄, formate, and ethanol (first stacked column Figure 3. B).
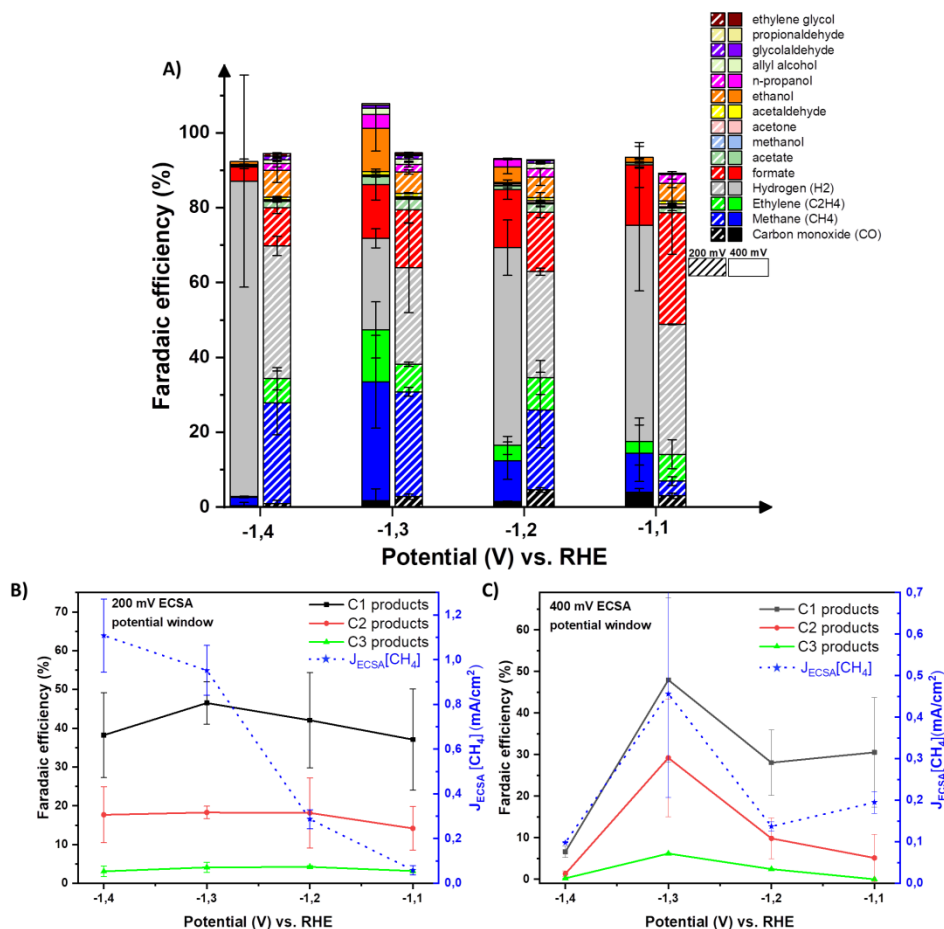
A)

Faradaic efficiency (%)

Potential (V) vs. RHE

Legend:
ethylene glycol
propionaldehyde
glycolaldehyde
allyl alcohol
n-propanol
ethanol
acetaldehyde
acetone
methanol
acetate
formate
Hydrogen (H2)
Ethylene (C2H4)
Methane (CH4)
Carbon monoxide (CO)

200 mV 400 mV

B) 200 mV ECSA potential window — C1 products, C2 products, C3 products, $J_{ECSA}[CH_4]$

Faradaic efficiency (%) / $J_{ECSA}[CH_4] (mA/cm^2)$ — Potential (V) vs. RHE

C) 400 mV ECSA potential window — C1 products, C2 products, C3 products, $J_{ECSA}[CH_4]$

Faradaic efficiency (%) / $J_{ECSA}[CH_4] (mA/cm^2)$ — Potential (V) vs. RHE

Figure 4. A) Potential-dependent Faradaic efficiency plots for Cu NCs-OCP200 (striped columns) and Cu NCs-OCP400 samples. FEs of C_1, C_2, and C_3 products at various potentials for B) Cu NCs-OCP200 and; C) Cu NCs-OCP400 samples.

Hydrogen, as an ever-present undesirable product in the CO_2RR, was the main product impacting 83% of total Faradaic efficiency. Given the high susceptibility to Cu NCs reconstruction under CO_2RR-relevant conditions[12,14,16], this was an indication that the initial (as-prepared) size, shape, and composition of the catalyst do not govern the final selectivity. The absence of significant change upon exposure only to the 0.1M $KHCO_3$ electrolyte, except for slight shrinking due to the reduction and dissolution, allowed us to refer to the performance of as-prepared Cu-based cubes (Figure S17 A). The facets' roughening and loss of the edge sharpness with substantial small redeposited nanoparticles ~5-10 nm after electrolysis also confirm previous findings by Reske *et al.*[41] where hydrogen evolution reaction (HER) is dominant on Cu nanoparticles with dimensions below 5nm (Figure S16. A). To further confirm the non-selectivity of as-prepared Cu NCs, we did the long-term electrolysis at -1.3 V vs. RHE for 10h. Even though, in the first 30 min of electrolysis Cu NCs showed some selectivity toward methane and ethylene at around 10% of faradaic efficiency (FE), after 1.5h of CO_2RR reaction time the FE dropped below 5% and remained throughout the whole reaction time of 10h. The HER dominates, as also shown for the 1h reaction, with a slight increase with time (Figure S16. B).

Therefore, we employed the double-layer capacitance method with two potential windows of 200 and 400 mV, with no breakup between EDLC-ECSA and CA measurements. The idea is to prevent the Cu surface from undergoing oxidation at OCP. This induces besides the addition of more oxygen in the Cu

NCs also its subsequent dissolution[42], where dissolved Cu ions can serve afterward for additional reconstruction through redeposition at an applied negative bias. Unlike the as-prepared Cu NCs exposed only to the electrolyte, we observed slight changes in the Cu nanocubes' morphology after only exposing them to the ECSA determination protocol (Figure S17 B, C). In both cases, the analysis of ex-situ SEM images reveals loss of facets' sharpness, roughness increment, and redeposition of small nanoparticles (NPs), where the process is shifted toward more positive potential (accounting for the end scan in the ECSA determination method of -0.7V vs. Ag/AgCl) than the potential reported by Grosse *et al.*[12] where re-deposited Cu NPs form right below -0.3 V_{RHE}. Nevertheless, even though the Cu NCs exhibited slight morphological changes due to the EDLC-ECSA treatment the selectivity remained similar to as-prepared Cu NCs. The marginal increase in CH_4 formation of Cu NCs-NOOCP200 and NOOCP400 samples reaching up to FE of 9% to the latter one was overshadowed by a dominant HER that exceeded 80% at -1.3V vs. RHE. Furthermore, we studied the Cu NCs at various potentials with 200 and 400 mV ECSA window range, whereas in the electrochemical protocol between EDLC-ECSA and CA measurements, Cu NCs were allowed to return to OCP. The fact that Cu NCs are further exposed to OCP at around +0.5V_{RHE}, leaves room for secondary dissolution after the first one when the electrolyte was introduced.[26] Figure 4. A shows the FEs of Cu-based NCs with a different employed ECSA window range apriori electrolysis from -1.1 to -1.4 V vs. RHE. Accordingly, to a previous notation, hereby, the samples are denoted as "Cu NCs-OCP200" and "Cu NCs-OCP400". At -1.1 V vs. RHE, both samples show activity for multiple products, where formate stands out as the predominant product with a top-high for all the studied potentials. A distinctive characteristic of C_1 products is the exchange in production of the formate and CH_4 by increasing overpotential, where at the lowest overpotential formate is dominant. Interestingly, this is the onset potential for methane (CH_4), with a considerable for Cu NCs-OCP400 of 10,5%. Even though both samples do not follow the same trend in CH_4 production by increasing reductive potential, they reach the best performance at -1.3V vs. RHE with FE_{CH4} of 28.0% and 31.7% for Cu NCs-OCP200 and Cu NCs-OCP400, respectively. Expectedly, the HER dominates for both samples at the highest overpotential of -1.4 V vs. RHE. Moreover, Figure 4. B and C represent the C_1, C_2, and C_3 products trend, and ECSA-normalized partial current densities for CH_4 for Cu NCs-OCP400 and Cu NCs-OCP200, respectively. Cu NCs-OCP200 sample tracks a mild volcano-shaped trend, with the highest selectivity towards CO_2RR products at -1.3V vs. RHE, whereas the prevalence of C_1 products leads to FE of 46.5%. However, the partial current for CH_4 does not follow the same trend, and it is increasing by increasing overpotential, reaching the highest observed current density for all samples of 1.108 mA/cm^2 at -1.4V vs. RHE. Worthnotly, Cu NCs-OCP200 shows to exchange C_1 products selectivity between peak potential at -1.3V and -1.1V, where at the latter one selectivity is foremost shifted towards the formate production. Cu NCs-OCP400 follows a similar trend, with a more prominent peak for all the products at -1.3 V vs. RHE. C_1 products ruled the selectivity at a peak potential reaching 49.0% with predominant methane production of FE_{CH4}=31.7%. In contrast to the 200 mV window width case, the Cu NCs-OCP400 sample follows an analogous trend for a partial current density of CH_4 as for C_1, C_2, and C_3 product distribution, with a twice reduced current density of 0.456 mA/cm^2 in comparison with Cu NCs-OCP200.

3.3. Morphological evolution under CO_2RR

The decent selectivity toward methane for both Cu NCs-OCP200 and Cu NCs-OCP400 samples at a peak potential of -1.3V vs. RHE, we further correlate with the ex-situ SEM before and after images. Figure 5. reveals different morphological motifs after 1h of electrolysis at the peak-selectivity potential of -1.3V vs RHE depending upon ECSA potential window with(out) exposure to the OCP in-between electrolysis step. Figures 5. A and B show the morphological evolution of the Cu NCs when the surfaces have not been exposed to the OCP after the ECSA determination step with 400 and
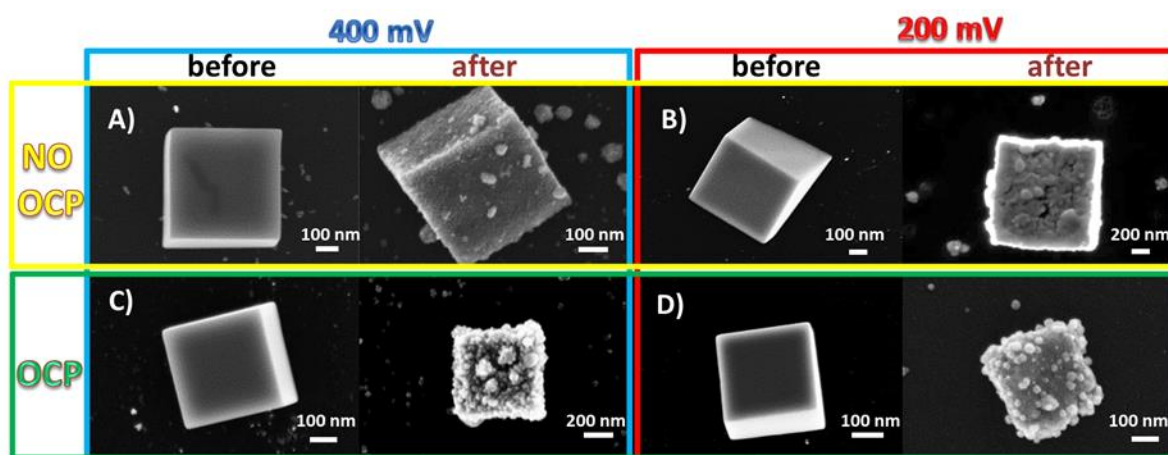
Figure 5. Different morphological evolution of Cu NCs with(out) exposure to OCP in-between ECSA and electrolysis based on ECSA potential window. All SEM after images were done after 1h electrolysis at -1,3 V_{RHE}. A) Cu NCs - NOOCP400 sample; B) Cu NCs – NOOCP200 sample; C) Cu NCs - OCP400 sample; D) Cu NCs – OCP200 sample.

200 mV potential windows, respectively. Pronounced roughness and moderate redeposition of NPs endorse structure-performance relationship as in the case for as-prepared Cu-based NCs. We posit that in both cases, the preservation of the abrupt morphological transformation and depletion of the near-surface oxygen leads to the Cu-rich surface formation that predominantly produces H_2.[43,44] However when the Cu-based NCs were exposed to the OCP in-between EDLC-ECSA measurements (Supplementary note 4) and static CO_2RR electrolysis further roughening and irreversible morphological transformation is noticeable. Figure 5. C and D display the morphological evolution of Cu NCs-OCP400 and Cu NCs-OCP200 samples, respectively. Considering that additional dissolution of Cu occurred by exposing the already distressed cubes to the OCP (Figure S17 B, C), the Cu ions served for intense reconstruction through the dissolution/redeposition process similar to the Ostwald ripening after applying negative bias.[22,24] The redeposited fragments in the range of 20-40 nm form highly granular morphology and increased the surface roughness for CuNCs-OCP400 samples. The redeposition can be observed also in the vicinity of the cubic particles. Hence, the evolved surface displays a more than threefold enhancement of CH_4 formation (FE_{CH4}=31%) compared to the Cu NCs-NOOCP400 sample. Likewise, Cu NCs-OCP200 has a similar morphological transformation with slightly alleviated redeposited fragments, but it is still highly granular, exhibiting again threefold enhancement with doubled partial current density relative to the Cu NCs-OCP400 sample.
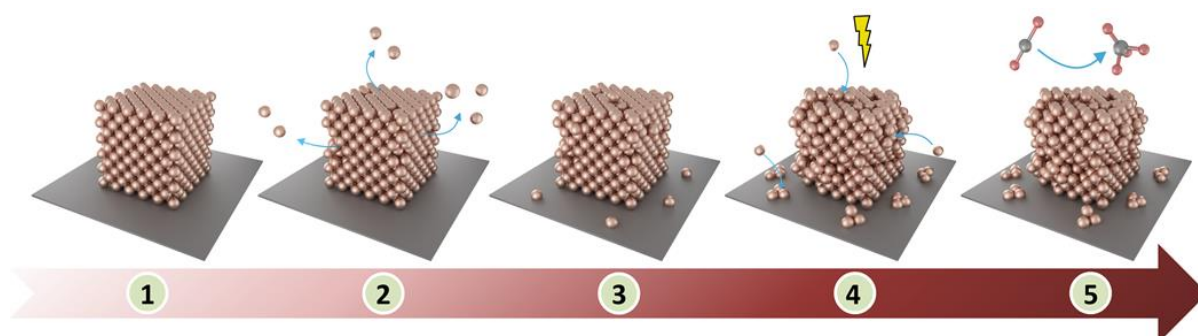

Figure 6. The schematic representation of the morphological and structural evolution of the Cu NCs during CO2RR. Step 1. as-prepared Cu NCs; Step 2. introduction of electrolyte dissolution of Cu24,42; Step 3. favorable reconstruction during double-layer cycling (ECSA determination); Step 4. negative applied bias: i) redeposition due to exposure to OCP after ECSA, ii) reduction of near-surface oxide, iii) CO2RR; Step 5. dynamically evolved surface – decent production of methane.

Our results are in alignment with the recent literature on Cu NCs, where Grosse *et al.*[9] emphasized the influence of support for favorable production of CH_4 on the Cu cubes on carbon support. Most recently, Timoshenko *et al.*[40] reported that enhancement in CH_4 production is attributed to the irreversible increase in surface roughness and granular morphology. Since Cu^0-dominated catalyst surfaces favoring the CH_4 have been demonstrated[27,45,46], we propose that the bulk Cu_2O core surrounded by a granular island/fragments of Cu^0 in the near-surface are the main active sites, that have been proposed to form in a few seconds after cathodic potential.[40] Considering all the above discussion, we posit the morphological and structural evolution of the electrochemically-grown Cu-based NCs on glassy carbon support for favorable CO_2 electroreduction to CH_4 through schematic representation as shown in Figure 6. As-synthesized Cu_2O nanocubes endure transformation immediately after the introduction of 0.1M $KHCO_3$ electrolyte (step 2), which is dissolution[24,42]. The EDLC-ECSA seems to have a positive influence on the lattice rearrangement (step 3), but favorable reconstruction occurs after exposing the Cu surface once again to OCP (additional dissolution). Hence, by applying a negative bias of -1.3 V vs. RHE when additional redeposition occurs, making Cu nanocube's surface highly granular with increased roughness (step 4). As a result of the highly granular morphology created during redeposition, combined with a higher surface roughness in Cu^0/Cu_2O composition, CH_4 is favorably produced (step 5). To sum up, the chloride-free ~500 nm Cu nanocubes are synthesized by a simple pulse-alternating electrodeposition method from a 0.01M $CuSO_4$ bath. We show that the determination method (double-layer cycling) of one of the critical parameters for reporting a catalyst's intrinsic activity, namely electrochemical surface area (ECSA), plays an important role as the initiator for the enhancement of catalytic reactivity of Cu-based NCs.

4. Conclusions

In this study, we successfully synthesized and characterized the electrochemically grown chloride-free Cu NCs on a glassy carbon substrate. Under the appropriate electrochemical protocol, which consists of electrochemical double-layer cycling and subsequent exposure to the OCP before electrolysis, the activity can be increased threefold for CO_2 to CH_4 conversion. The maximum Faradaic efficiency of 31.7% of CH_4 is achieved due to the formation of highly granular morphology with increased surface roughness with most probably Cu^0/Cu_2O composition, which is in agreement with the current in-situ studies.[40] To further elaborate on the preferential selectivity toward methane on Cl^--free Cu NCs, we noticed the positive effect of chloride anions on the CO chemisorption (stabilization) on the copper surface according to the DFT calculations (see Supplementary note 7), which was previously proposed for the formation of C_3-C_4 products in the study of Seunghwa *et al.*[47] As well as in our previous studies[16,22], we stress a practical note of Cu NCs catalyst favorable reconstruction under mentioned conditions, which can mimic the operation of CO_2RR electrolyzer under the start/stop conditions.

Authorship contribution statement

S.P. had a major contribution. M.A.N. had the second most contribution, with involvement in the nanocubes characterization, electrocatalytic measurements, DFT calculations as well as writing supervision. P.Š. established an NMR protocol for liquid product detection. L.S. contributed to the design and construction of the sandwich-type electrochemical cell. K.M.K, B.L., L.P., A.K.S., and M.B. contributed equally. N.H. conceived and supervised the project. All authors have approved the final version of the manuscript**.**

Declaration of Competing Interest

The authors declare that they have no known competing financial interests or personal relationships that could have appeared to influence the work reported in this paper.

Data Availability

Data available on request from the interested.

Acknowledgments

Supplementary materials

Supplementary material associated with this article can be found, in the online version, at xxxxxx

Includes, the synthesis of Cu_2O nanocubes (Cu NCs) –floating method; Influence of the stirring rate of electrolyte; Chloride effect on the synthesis of Cu NCs; Tuning electrochemical protocol to control the size of Cu NCs; XPS measurements of as-prepared Cu NCs; XRD measurements of as-prepared Cu NCs; Raman measurements of as-prepared Cu NCs; The electrochemical custom-made cell configuration; Electrochemical surface area determination: Electrocatalytic measurements and products detection; Electrocatalytic performance of as-prepared Cu NCs; Morphological evolution of Cu NCs; Effect of specifically adsorbed chloride anions.

References

[1]   H.D. Yoo, E. Markevich, G. Salitra, D. Sharon, D. Aurbach, On the challenge of developing advanced technologies for electrochemical energy storage and conversion, Mater. Today. 17 (2014) 110–121. doi:10.1016/j.mattod.2014.02.014.

[2]   D. Pletcher, Electrochemistry Communications The cathodic reduction of carbon dioxide — What can it realistically achieve ? A mini review, Electrochem. Commun. 61 (2015) 97–101. doi:10.1016/j.elecom.2015.10.006.

[3]   S.A. Nitopi, E. Bertheussen, S.B. Scott, X. Liu, K. Albert, S. Horch, B. Seger, I.E.L. Stephens, K. Chan, J.K. Nørskov, T.F. Jaramillo, I. Chorkendorff, Progress and Perspectives of Electrochemical CO 2 Reduction on Copper in Aqueous Electrolyte, Chem. Rev. (2018). doi:10.1021/ACS.CHEMREV.8B00705.

[4]   M. Gattrell, N. Gupta, A. Co, A review of the aqueous electrochemical reduction of CO2 to hydrocarbons at copper, J. Electroanal. Chem. (2006). doi:10.1016/j.jelechem.2006.05.013.

[5]   K. Rossi, R. Buonsanti, Shaping Copper Nanocatalysts to Steer Selectivity in the Electrochemical CO2 Reduction Reaction, Acc. Chem. Res. 55 (2022) 629–637. doi:10.1021/acs.accounts.1c00673.

[6]   Y. Hori, I. Takahashi, O. Koga, N. Hoshi, Electrochemical reduction of carbon dioxide at various series of copper single crystal electrodes, J. Mol. Catal. A Chem. 199 (2003) 39–47. doi:10.1016/S1381-1169(03)00016-5.

[7]   Y. Hori, I. Takahashi, O. Koga, N. Hoshi, Selective formation of C2 compounds from electrochemical reduction of CO2 at a series of copper single crystal electrodes, J. Phys. Chem. B. 106 (2002) 15–17. doi:10.1021/jp013478d.

[8]   F.S. Roberts, K.P. Kuhl, A. Nilsson, High selectivity for ethylene from carbon dioxide reduction over copper nanocube electrocatalysts, Angew. Chemie - Int. Ed. 54 (2015) 5179–5182. doi:10.1002/anie.201412214.

[9]   P. Grosse, D. Gao, F. Scholten, I. Sinev, H. Mistry, B. Roldan Cuenya, Dynamic Changes in the Structure, Chemical State and Catalytic Selectivity of Cu Nanocubes during CO 2 Electroreduction: Size and Support Effects, Angew. Chemie - Int. Ed. (2018). doi:10.1002/anie.201802083.

[10]   G. Mangione, J. Huang, R. Buonsanti, C. Corminboeuf, Dual-Facet Mechanism in Copper Nanocubes for Electrochemical CO 2 Reduction into Ethylene , J. Phys. Chem. Lett. 10 (2019) 4259–4265. doi:10.1021/acs.jpclett.9b01471.

[11]   T. Möller, F. Scholten, T.N. Thanh, I. Sinev, J. Timoshenko, X. Wang, Z. Jovanov, M. Gliech, B. Roldan Cuenya, A.S. Varela, P. Strasser, Electrocatalytic CO2 Reduction on CuOx Nanocubes: Tracking the Evolution of Chemical State, Geometric Structure, and Catalytic Selectivity using Operando Spectroscopy, Angew. Chemie - Int. Ed. (2020). doi:10.1002/anie.202007136.

[12]   P. Grosse, A. Yoon, C. Rettenmaier, A. Herzog, S.W. Chee, B. Roldan Cuenya, Dynamic transformation of cubic copper catalysts during CO2 electroreduction and its impact on catalytic selectivity, Nat. Commun. 12 (2021) 1–11. doi:10.1038/s41467-021-26743-5.

[13]   U.S. Mohanty, Electrodeposition: A versatile and inexpensive tool for the synthesis of nanoparticles, nanorods, nanowires, and nanoclusters of metals, J. Appl. Electrochem. 41 (2011) 257–270. doi:10.1007/s10800-010-0234-3.

[14]   R.M. Arán-Ais, R. Rizo, P. Grosse, G. Algara-Siller, K. Dembélé, M. Plodinec, T. Lunkenbein, S.W. Chee, B.R. Cuenya, Imaging electrochemically synthesized Cu2O cubes and their morphological evolution under conditions relevant to CO2 electroreduction, Nat. Commun. (2020). doi:10.1038/s41467-020-17220-6.

[15]   A. Loiudice, P. Lobaccaro, E.A. Kamali, T. Thao, B.H. Huang, J.W. Ager, R. Buonsanti, Tailoring Copper Nanocrystals towards C2 Products in Electrochemical CO2 Reduction, Angew. Chemie - Int. Ed. 55 (2016) 5789–5792. doi:10.1002/anie.201601582.

[16]   S. Popović, M. Smiljanić, P. Jovanovič, J. Vavra, R. Buonsanti, N. Hodnik, Stability and Degradation Mechanisms of Copper-Based Catalysts for Electrochemical CO2 Reduction, Angew. Chemie - Int. Ed. (2020). doi:10.1002/anie.202000617.

[17]   J. Huang, N. Hörmann, E. Oveisi, A. Loiudice, G.L. De Gregorio, O. Andreussi, N. Marzari, R. Buonsanti, Potential-induced nanoclustering of metallic catalysts during electrochemical CO2 reduction, Nat. Commun. 9 (2018) 1–9. doi:10.1038/s41467-018-05544-3.

[18]   P. Wilde, P.B. O'Mara, J.R.C. Junqueira, T. Tarnev, T.M. Benedetti, C. Andronescu, Y.T. Chen, R.D. Tilley, W. Schuhmann, J.J. Gooding, Is Cu instability during the CO2reduction reaction governed by the applied potential or the local CO concentration?, Chem. Sci. 12 (2021) 4028–4033. doi:10.1039/d0sc05990k.

[19]   A.S. Varela, M. Kroschel, T. Reier, P. Strasser, Controlling the selectivity of CO2 electroreduction on copper: The effect of the electrolyte concentration and the importance of the local pH, Catal. Today. 260 (2016) 8–13. doi:10.1016/j.cattod.2015.06.009.

[20]   J. Wang, H. Chen, H. Tan, C.M. Tan, Y. Zhu, H.M. Chen, Strong Correlation between the Dynamic Chemical State and Product Pro fi le of Carbon Dioxide Electroreduction, (2022). doi:10.1021/acsami.1c19380.

[21]   G.H. Simon, C.S. Kley, B. Roldan Cuenya, Potential-Dependent Morphology of Copper Catalysts During CO 2 Electroreduction Revealed by In Situ Atomic Force Microscopy , Angew. Chemie Int. Ed. (2020). doi:10.1002/anie.202010449.

[22]   S. Popovic, M. Bele, N. Hodnik, Reconstruction of Copper Nanoparticles at Electrochemical CO2 Reduction Reaction Conditions Occurs via Two-step Dissolution/Redeposition Mechanism, ChemElectroChem. 8 (2021) 2634–2639. doi:10.1002/celc.202100387.

[23]   S.J. Raaijman, N. Arulmozhi, M.T.M. Koper, Morphological Stability of Copper Surfaces under Reducing Conditions, ACS Appl. Mater. Interfaces. 13 (2021) 48730–48744. doi:10.1021/acsami.1c13989.

[24]   J. Vavra, T. Shen, D. Stoian, V. Tileli, R. Buonsanti, Real-time Monitoring Reveals Dissolution/Redeposition Mechanism in Copper Nanocatalysts during the Initial Stages of the CO 2 Reduction Reaction , Angew. Chemie Int. Ed. (2020). doi:10.1002/anie.202011137.

[25]   S. Yu, S. Louisia, P. Yang, The Interactive Dynamics of Nanocatalyst Structure and Microenvironment during Electrochemical CO 2 Conversion, (2022). doi:10.1021/jacsau.1c00562.

[26]   J. Vavra, F. Dattila, A. Kormányos, S. Cherevko, N. Lopéz, Cu + transient species mediate Cu catalyst reconstruction during CO 2 electroreduction, (1950).

[27]   C.J. Chang, S.C. Lin, H.C. Chen, J. Wang, K.J. Zheng, Y. Zhu, H.M. Chen, Dynamic Reoxidation/Reduction-Driven Atomic Interdiffusion for Highly Selective CO2Reduction toward Methane, J. Am. Chem. Soc. 142 (2020) 12119–12132. doi:10.1021/jacs.0c01859.

[28]   S.Y. Lee, H. Jung, N.K. Kim, H.S. Oh, B.K. Min, Y.J. Hwang, Mixed Copper States in Anodized Cu Electrocatalyst for Stable and Selective Ethylene Production from CO 2 Reduction, J. Am. Chem. Soc. 140 (2018) 8681–8689. doi:10.1021/jacs.8b02173.

[29]   P. Chauhan, K. Hiekel, J.S. Diercks, J. Herranz, V.A. Saveleva, P. Khavlyuk, A. Eychmüller, T.J. Schmidt, Electrochemical Surface Area Quantification, CO 2 Reduction Performance, and Stability

Studies of Unsupported Three-Dimensional Au Aerogels versus Carbon-Supported Au Nanoparticles , ACS Mater. Au. (2022). doi:10.1021/acsmaterialsau.1c00067.

[30]   O.A. Baturina, Q. Lu, M.A. Padilla, L. Xin, W. Li, A. Serov, K. Artyushkova, P. Atanassov, F. Xu, A. Epshteyn, T. Brintlinger, M. Schuette, G.E. Collins, CO2 electroreduction to hydrocarbons on carbon-supported Cu nanoparticles, ACS Catal. (2014). doi:10.1021/cs500537y.

[31]   H. Mistry, R. Reske, Z. Zeng, Z.J. Zhao, J. Greeley, P. Strasser, B.R. Cuenya, Exceptional size-dependent activity enhancement in the electroreduction of CO2 over Au nanoparticles, J. Am. Chem. Soc. 136 (2014) 16473–16476. doi:10.1021/ja508879j.

[32]   Y. Hori, H. Konishi, T. Futamura, A. Murata, O. Koga, H. Sakurai, K. Oguma, "deactivation of copper electrode" in electrochemical reduction of CO 2, Electrochim. Acta. (2005). doi:10.1016/j.electacta.2005.03.015.

[33]   A. Fateh, M. Aliofkhazraei, A.R. Rezvanian, Review of corrosive environments for copper and its corrosion inhibitors, Arab. J. Chem. (2020). doi:10.1016/j.arabjc.2017.05.021.

[34]   C. Wei, S. Sun, D. Mandler, X. Wang, S.Z. Qiao, Z.J. Xu, Approaches for measuring the surface areas of metal oxide electrocatalysts for determining their intrinsic electrocatalytic activity, Chem. Soc. Rev. 48 (2019) 2518–2534. doi:10.1039/c8cs00848e.

[35]   M.B. Gawande, A. Goswami, F.X. Felpin, T. Asefa, X. Huang, R. Silva, X. Zou, R. Zboril, R.S. Varma, Cu and Cu-Based Nanoparticles: Synthesis and Applications in Catalysis, Chem. Rev. 116 (2016) 3722–3811. doi:10.1021/acs.chemrev.5b00482.

[36]   P. Grosse, A. Yoon, C. Rettenmaier, S.W. Chee, B.R. Cuenya, Growth Dynamics and Processes Governing the Stability of Electrodeposited Size-Controlled Cubic Cu Catalysts, J. Phys. Chem. C. 124 (2020) 26908–26915. doi:10.1021/acs.jpcc.0c09105.

[37]   E. Howe, ENGINEERING CHEMISTRY Chemical Analysis by X-Ray Diffraction, Ind. Eng. Chem. - Anal. Ed. 10 (1938) 457–506.

[38]   Y. Petroff, P.Y. Yu, Y.R. Shen, Study of photoluminescence in ${\mathrm{Cu}}_{2}$O, Phys. Rev. B. 12 (1975) 2488–2495. doi:10.1103/PhysRevB.12.2488.

[39]   L. Yang, J. Lv, Y. Sui, W. Fu, X. Zhou, J. Ma, S. Su, W. Zhang, P. Lv, D. Wu, Y. Mu, H. Yang, Fabrication of Cu2O/Ag composite nanoframes as surface-enhanced Raman scattering substrates in a successive one-pot procedure, CrystEngComm. 16 (2014) 2298–2304. doi:10.1039/c3ce42052c.

[40]   J. Timoshenko, A. Bergmann, C. Rettenmaier, A. Herzog, R.M. Arán-Ais, H.S. Jeon, F.T. Haase, U. Hejral, P. Grosse, S. Kühl, E.M. Davis, J. Tian, O. Magnussen, B. Roldan Cuenya, Steering the structure and selectivity of CO2 electroreduction catalysts by potential pulses, Nat. Catal. 5 (2022) 259–267. doi:10.1038/s41929-022-00760-z.

[41]   R. Reske, H. Mistry, F. Behafarid, B. Roldan Cuenya, P. Strasser, Particle size effects in the catalytic electroreduction of CO2 on Cu nanoparticles, J. Am. Chem. Soc. 136 (2014) 6978–6986. doi:10.1021/ja500328k.

[42]   F.D. Speck, S. Cherevko, Electrochemical copper dissolution: A benchmark for stable CO2 reduction on copper electrocatalysts, Electrochem. Commun. (2020). doi:10.1016/j.elecom.2020.106739.

[43]   S.H. Lee, J.C. Lin, M. Farmand, A.T. Landers, J.T. Feaster, J.E. Avilés Acosta, J.W. Beeman, Y. Ye, J. Yano, A. Mehta, R.C. Davis, T.F. Jaramillo, C. Hahn, W.S. Drisdell, Oxidation State and Surface Reconstruction of Cu under CO2Reduction Conditions from in Situ X-ray Characterization, J. Am. Chem. Soc. 143 (2021) 588–592. doi:10.1021/jacs.0c10017.

[44]   G. Liu, M. Lee, S. Kwon, G. Zeng, J. Eichhorn, A.K. Buckley, F.D. Toste, W.A. Goddard, F.M. Toma, CO2 reduction on pure Cu produces only H2 after subsurface O is depleted: Theory and experiment, Proc. Natl. Acad. Sci. U. S. A. 118 (2021). doi:10.1073/pnas.2012649118.

[45]   D. Kim, S. Lee, J.D. Ocon, B. Jeong, J.K. Lee, J. Lee, Insights into an autonomously formed oxygen-evacuated Cu2O electrode for the selective production of C2H4 from CO2, Phys. Chem. Chem. Phys. 17 (2015) 824–830. doi:10.1039/c4cp03172e.

[46]   H. Mistry, A.S. Varela, C.S. Bonifacio, I. Zegkinoglou, I. Sinev, Y.W. Choi, K. Kisslinger, E.A. Stach, J.C. Yang, P. Strasser, B.R. Cuenya, Highly selective plasma-activated copper catalysts for carbon dioxide reduction to ethylene, Nat. Commun. (2016). doi:10.1038/ncomms12123.

[47]   S. Lee, D. Kim, J. Lee, Electrocatalytic Production of C3-C4 Compounds by Conversion of CO 2 on a Chloride-Induced Bi-Phasic Cu 2 O-Cu Catalyst , Angew. Chemie. 127 (2015) 14914–14918. doi:10.1002/ange.201505730.

Highlights:

- ➢ Electrodeposition of chloride-free Cu NCs
- ➢ Activation of Cu NCs by appropriate electrochemical protocol
- ➢ Support effect towards the selective formation of methane on Cu NCs
- ➢ Influence of electrochemical double layer cycling and OCP in tuning the activity and selectivity of Cu NCs

Graphical abstract: